

Phase diagram and Hall effect of the electron doped manganite $\text{La}_{1-x}\text{Ce}_x\text{MnO}_3$

P. Raychaudhuri^{a)}

School of Physics and Astronomy, University of Birmingham, Edgbaston, Birmingham, B15 2TT, United Kingdom and School of Physics and Astronomy, University of St. Andrews, North Haugh, St. Andrews, KY16 9SS, United Kingdom

C. Mitra

Department of Materials Science, University of Cambridge, Pembroke St, Cambridge CB2 3QZ, United Kingdom

P. D. A. Mann

School of Physics and Astronomy, University of St. Andrews, North Haugh, St. Andrews, KY16 9SS, United Kingdom

S. Wirth^{b)}

MPI for Chemical Physics of Solids, Nöthnitzerstr. 40, D-01187 Dresden, Germany

(Presented on 15 November 2002)

We report on the electronic, transport, and magnetic properties of the Ce-doped manganite, $\text{La}_{1-x}\text{Ce}_x\text{MnO}_3$. This material is remarkably similar to the heavily investigated hole doped manganite $\text{La}_{1-x}\text{Ca}_x\text{MnO}_3$; e.g., both materials show Curie temperatures of $T_C \sim 250$ K for $x = 0.3$. The main difference which makes the Ce-doped material highly interesting for basic research as well as for possible applications (e.g., in spintronics) is the fact that Ce doping drives the manganese in a mixture of Mn^{2+} and Mn^{3+} induced by electron doping. We present conclusive evidence for electron doping by x-ray absorption spectroscopy and Hall measurements on single phase epitaxial thin films. From transport measurements on a series of $\text{La}_{1-x}\text{Ce}_x\text{MnO}_3$, the magnetic phase diagram of $\text{La}_{1-x}\text{Ce}_x\text{MnO}_3$ is established. © 2003 American Institute of Physics. [DOI: 10.1063/1.1556976]

I. INTRODUCTION

Mixed valence manganese oxides $\text{R}_{1-x}\text{A}_x\text{MnO}_3$ (R = rare-earth cation, A = alkali or alkaline earth cation) have been heavily investigated in recent years.^{1,2} They show a variety of interesting crystallographic, electronic, and magnetic properties, one of which is the magnetoresistance. The latter effect may become extraordinarily large (so-called colossal magnetoresistance) for temperatures around the ferromagnetic transition temperature T_C . Below T_C the mixed valence manganites most commonly behave as ferromagnetic metals. This behavior becomes obvious, e.g., if trivalent La in the parent compound LaMnO_3 is substituted by divalent Ca: the missing electron produces a hole by driving the Mn^{3+} into the Mn^{4+} state. The crystal field interactions split the 5 *d* orbitals of Mn into 3 t_{2g} and 2 e_g orbitals. Hence, the e_g orbital is occupied by one electron in case of Mn^{3+} and is empty for Mn^{4+} which makes the former subject to Jahn–Teller distortion whereas the latter is not.

From the aforementioned point of view one may ask whether it is also possible to induce electron doping by substitution of R by a tetravalent element A. Having both electron as well as hole doped ferromagnetic manganites may

open up very interesting applications in the emerging field of spintronics. However, a number of issues have to be addressed first: (i) Can any of the manganites containing a usually tetravalent element be prepared in single crystalline form? (ii) Does the considered element really drive the Mn in a 2+ valence state, i.e., induce electron doping? (iii) What are the main features of the magnetic phase diagram of the resulting compound? The latter issue is of special importance because of the known dependencies of the magnetic properties of the manganites on the doping x and the relative cation size R/A for divalent A, i.e., the hole doped manganites.³

It should be pointed out that Mn^{2+} and Mn^{4+} ions behave very similarly. Strong electron-phonon coupling was shown to be a necessary ingredient for explaining the magnetic and transport properties of the hole doped manganites.⁴ Both ions do *not* induce Jahn–Teller distortions whereas Mn^{3+} does. Hence, one might expect similarly interesting physics in the electron doped manganites as in their highly investigated hole doped counterparts.

In the following we report on the Ce-doped manganite, $\text{La}_{1-x}\text{Ce}_x\text{MnO}_3$. This material has been reported to be a good candidate to induce electron doping on the manganese site.^{5,6} We will summarize the evidence for this electron doping including Hall effect measurements. The magnetic phase diagram for $\text{La}_{1-x}\text{Ce}_x\text{MnO}_3$ with $0 \leq x \leq 0.3$ is presented. As a prerequisite, the preparation of single phase material in the thin film form is discussed. A detailed understanding of the

^{a)}Present address: Tata Institute of Fundamental Research, Homi Bhabha Road, Colaba, Mumbai 400 005, India.

^{b)}Author to whom correspondence should be addressed; electronic mail: wirth@cpfs.mpg.de

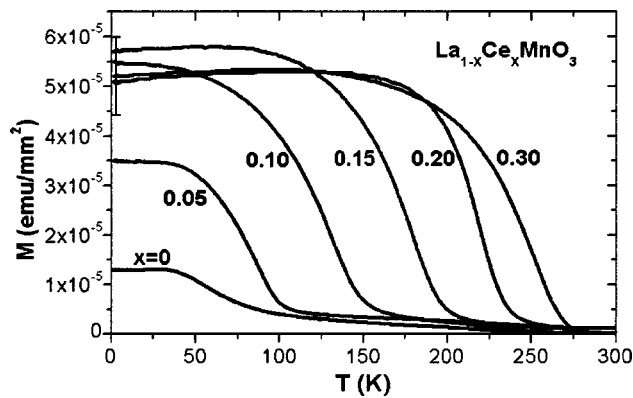


FIG. 1. Temperature dependence of the magnetization of thin film samples $\text{La}_{1-x}\text{Ce}_x\text{MnO}_3$ with $0 \leq x \leq 0.3$. The nominal Ce-doping x for the different samples is indicated. An error bar for the sample with $x=0.3$ at low temperature is shown.

electronic and magnetic properties is essential for further utilization of this material.

II. PREPARATION AND MEASUREMENTS

The precursor material $\text{La}_{1-x}\text{Ce}_x\text{MnO}_3$ with $0 \leq x \leq 0.3$ was prepared by a solid state reaction route^{7,8} and used as targets in the subsequent pulsed laser deposition. For the latter a KrF excimer laser with an energy density of about 3 J/cm² at a wavelength of 248 nm and a repetition rate of 10 Hz was used. Thin epitaxial films were deposited on LaAlO_3 substrates which were held at temperatures between 790 and 800 °C. During film growth the oxygen pressure inside the deposition chamber was kept at 100 mTorr. This low oxygen pressure was used in order to avoid over oxygenation of the manganite films (it is well known that excess oxygen induces hole doping). X-ray analysis (as reported in Refs. 7, 8) was conducted to ensure the single phase nature of the films.

It should be emphasized that finding the exact deposition parameters is crucial for the fabrication of single phase films. The target material is vaporized by the high-energy laser beam and must impinge onto the substrate before it thermalizes. Hence, the film quality depends sensitively on such parameters as, e.g., the target-substrate distance.

The sample magnetization was measured by using a Quantum Design superconducting quantum interference device. Subsequently, the films were patterned into Hall bars for transport measurements by photolithography and wet chemical etching. This also enabled a film thickness determination, $d \approx 50$ nm, by atomic force microscopy.

The magnetization measurements for $\text{La}_{1-x}\text{Ce}_x\text{MnO}_3$ for $0 \leq x \leq 0.3$ are summarized in Fig. 1. The evolution of the magnetic moment M as well as of T_C is evident. These data emphasize the high quality of the films.

III. EVIDENCE FOR ELECTRON DOPING

It is well known that Ce can exist in two valence states, Ce^{3+} and Ce^{4+} , and, therefore, we first need to establish that Ce substitution indeed induces electron doping. For the latter, first evidence was obtained⁹ by x-ray absorption spectroscopy (XAS) on thin films of $\text{La}_{0.7}\text{Ce}_{0.3}\text{MnO}_3$. XAS at the

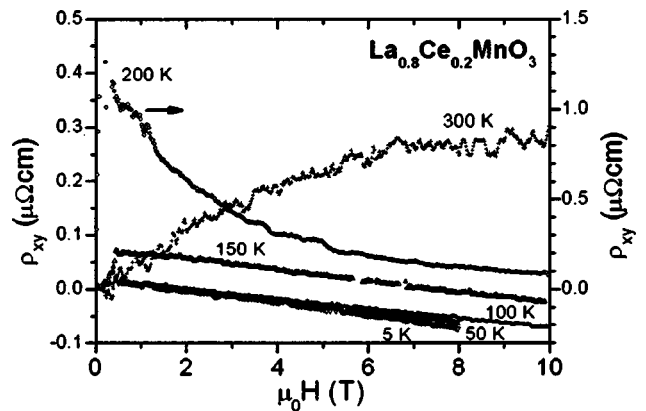


FIG. 2. Hall resistivity of the sample $\text{La}_{0.8}\text{Ce}_{0.2}\text{MnO}_3$ at different temperatures (as indicated by the labels). The curves for $T=5, 50, 100, 150$ and 300 K belong to the left scale, whereas the one for $T=200$ K is drawn compressed by a factor of 3 (right scale).

rare-earth $M_{4,5}$ and 3d transition metal $L_{2,3}$ threshold is known to be highly sensitive to valence states. The Ce- $M_{4,5}$ XAS spectrum of $\text{La}_{0.7}\text{Ce}_{0.3}\text{MnO}_3$ was compared to those of trivalent (CeF_3) and tetravalent (CeO_2) reference materials. For the investigated sample $\text{La}_{0.7}\text{Ce}_{0.3}\text{MnO}_3$, a pure Ce(IV) valence state was evident. In addition, Mn- $L_{2,3}$ spectra of $\text{La}_{0.7}\text{Ce}_{0.3}\text{MnO}_3$ were measured and compared to MnO (Mn^{2+}), LaMnO_3 (Mn^{3+}), and MnO_2 (Mn^{4+}) references. This procedure ensures that the electrons induced by Ce doping indeed drive a corresponding amount of Mn into a Mn^{2+} valence state. For our sample $\text{La}_{0.7}\text{Ce}_{0.3}\text{MnO}_3$ the spectrum clearly showed a mixture of Mn^{2+} and Mn^{3+} . The content of Mn^{2+} was estimated to about 20%. The lower Mn^{2+} content compared to the nominal 30% Ce doping could be caused by a slight over oxygenation of the sample.

Magnetoresistivity and Hall measurements were conducted on the metallic-like samples $x=0.15, 0.20$, and 0.30 for temperatures 5–300 K. Figure 2 shows the Hall resistivity of $\text{La}_{0.8}\text{Ce}_{0.2}\text{MnO}_3$ in dependence on the applied field H . Note that the curve measured at $T=200$ K was drawn using a compressed (right, factor of 3) scale. As the most important result, all curves measured at $T < T_C$ show a negative high-field slope, i.e., the main charge carriers are electrons.

In ferromagnetic thin films, the Hall resistivity is given by $\rho_{xy} = \mu_0(R_H H + R_S M)$ with R_H and R_S being the normal and anomalous (extraordinary) Hall coefficient.¹⁰ Assuming the simple case of a spherical Fermi surface with only one type of charge carrier, $R_H = 1/ne$. The resulting electron concentration n_e is shown in Fig. 3(a) in dependence on T/T_C . The increasing low- T value of n_e with increasing x may be related to the higher doping level. However, the absolute values of n_e are much larger than expected from the nominal doping. This situation is very similar to the Ca-doped manganites^{11–13} where it is discussed in terms of charge carrier compensation due to a majority spin band consisting of hole and electron Fermi surfaces.¹⁴ In general, the expression for R_H becomes rather complicated for nonspherical Fermi surfaces and if both types of charge carriers are present; also the mobilities need to be known. As an additional complication, the carriers in the Ce-doped manganites are minority

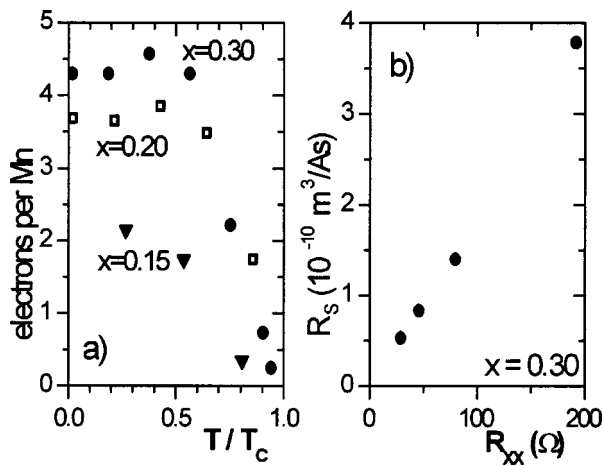


FIG. 3. (a) Scaled temperature dependence of the charge carrier concentration as determined from $n = 1/eR_H$ for the metallic samples, $x = 0.15, 0.20$ and 0.30 . (b) Anomalous Hall coefficient vs longitudinal resistance R_{xx} for sample $\text{La}_{0.7}\text{Ce}_{0.3}\text{MnO}_3$.

spin carriers.^{15,16} The essential finding of electrons as the dominating charge carriers is not affected.

As T is increased to approach T_C , the slope of ρ_{xy} becomes field dependent which cannot be explained by the anomalous Hall effect. For T close to T_C , we observed sign changes in $\rho_{xy}(H)$ for the samples $x = 0.15, 0.20$ and 0.30 (not shown). This emphasizes that a simple analysis $R_H = 1/ne$ is not valid and multiple bands at the Fermi level have to be considered. Above T_C , the large magnetoresistance and polaronic contributions are expected to influence ρ_{xy} . Here, higher fields are needed to decide whether the latter are electron-like as in the Ca-doped manganites.¹⁷

In ferromagnetic metals, R_S is expected to be proportional to the longitudinal resistance R_{xx} in the case of classical skew scattering. A linear relationship, $R_S \propto R_{xx}$ is found in the hole doped manganites.¹³ The scattering mechanism appears to be very similar in the hole and electron doped manganites since $R_S \propto R_{xx}$ also holds in $\text{La}_{1-x}\text{Ce}_x\text{MnO}_3$; an example is shown in Fig. 3(b) for $\text{La}_{0.7}\text{Ce}_{0.3}\text{MnO}_3$.

IV. PHASE DIAGRAM OF $\text{La}_{1-x}\text{Ce}_x\text{MnO}_3$

From the magnetization and resistance measurements the phase diagram of $\text{La}_{1-x}\text{Ce}_x\text{MnO}_3$ is constructed, see Fig. 4. The transition temperature between the ferromagnetic (FM) and the paramagnetic state is determined from T_C (marked by Δ) as well as from temperature T_p (\times in Fig. 4) at which R_{xx} assumes its maximum in case of the metallic samples. At low temperatures, i.e., in their ground state, samples with nominal doping $x \leq 0.10$ behave as ferromagnetic insulators whereas doping $x \geq 0.15$ results in FM metallic materials. This phase diagram is fascinatingly similar to the one reported for the Ca-doped manganite;³ a similarity that could not be expected due to the different ionic radii of Ca and Ce.

In conclusion, we reported on the magnetic and transport properties of $\text{La}_{1-x}\text{Ce}_x\text{MnO}_3$ with $0 \leq x \leq 0.30$. Conclusive

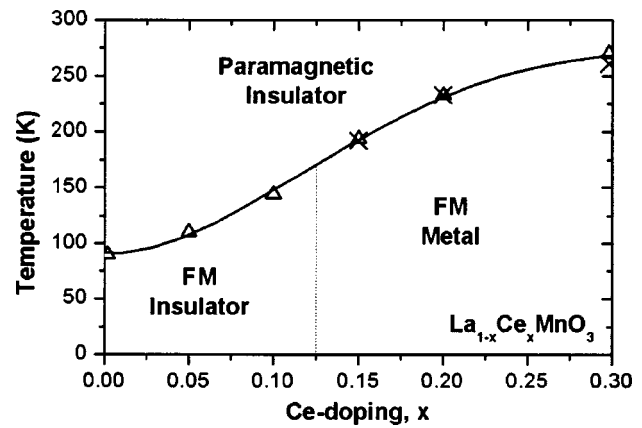


FIG. 4. Magnetic phase diagram of $\text{La}_{1-x}\text{Ce}_x\text{MnO}_3$ in the doping range $0 \leq x \leq 0.3$. The transition from ferromagnetic (FM) to paramagnetic behavior was determined from $T_C(\Delta)$ as well as from the temperature $T_p(\times)$ at which the maximum resistivity of the metallic samples occurs. Note the striking similarity of the phase diagrams for Ce- and Ca-doped manganites.

evidence for electron doping in these materials, at least for $0.15 \leq x \leq 0.30$, is presented. Having an electron-doped ferromagnetic counterpart to the well-known hole doped manganites opens up a vast field of possibilities for applications and research alike. Ferromagnetic junction devices^{15,16} may be conceivable for *spintronics* applications.

ACKNOWLEDGMENTS

P.R. wishes to acknowledge the Leverhulme Trust for financial support. S.W. wishes to express his gratitude to Professor F. Steglich.

- ¹S. Jin, T. H. Tiefel, M. McCormack, R. A. Fastnacht, R. Ramesh, and L. H. Chen, *Science* **264**, 413 (1994).
- ²J. M. D. Coey, M. Viret, and S. von Molnár, *Adv. Phys.* **48**, 167 (1999).
- ³P. Schiffer, A. P. Ramirez, W. Bao, and S.-W. Cheong, *Phys. Rev. Lett.* **75**, 3336 (1995).
- ⁴A. J. Millis, P. B. Littlewood, and B. I. Shraiman, *Phys. Rev. Lett.* **74**, 5144 (1995).
- ⁵P. Mandal and S. Das, *Phys. Rev. B* **56**, 15073 (1997).
- ⁶C. Mitra, P. Raychaudhuri, G. Köbernik, K. Dörr, K.-H. Müller, L. Schultz, and R. Pinto, *Appl. Phys. Lett.* **79**, 2408 (2001).
- ⁷P. Raychaudhuri, S. Mukherjee, A. K. Nigam, J. John, U. D. Vaisnav, R. Pinto, and P. Mandal, *J. Appl. Phys.* **86**, 5718 (1999).
- ⁸C. Mitra, P. Raychaudhuri, J. John, S. K. Dhar, A. K. Nigam, and R. Pinto, *J. Appl. Phys.* **89**, 524 (2001).
- ⁹C. Mitra, Z. Hu, P. Raychaudhuri, S. Wirth, S. I. Osiszar, H. H. Hsieh, H.-J. Lin, C. T. Chen, and L. H. Tjeng, *Phys. Rev. B* (in press).
- ¹⁰C. M. Hurd, *The Hall Effect in Metals and Alloys* (Plenum, New York, 1972).
- ¹¹P. Matl, N. P. Ong, Y. F. Yan, Y. Q. Li, D. Studebaker, T. Baum, and G. Doubinina, *Phys. Rev. B* **57**, 10248 (1998).
- ¹²G. Jacob, F. Martin, W. Westerburg, and H. Adrian, *Phys. Rev. B* **57**, 10252 (1998).
- ¹³S. H. Chun, M. B. Salomon, and P. D. Han, *J. Appl. Phys.* **85**, 5573 (1999).
- ¹⁴W. E. Pickett and D. J. Singh, *Phys. Rev. B* **53**, 1146 (1996).
- ¹⁵C. Mitra, G. Köbernik, K. Dörr, K. H. Müller, L. Schultz, P. Raychaudhuri, R. Pinto, and E. Wieser, *J. Appl. Phys.* **91**, 7715 (2002).
- ¹⁶C. Mitra, P. Raychaudhuri, K. Dörr, K.-H. Müller, L. Schultz, P. M. Openeer, and S. Wirth, *Phys. Rev. Lett.* **90**, 017202 (2003).
- ¹⁷M. Jaime, H. T. Hardner, M. B. Salomon, M. Rubinstein, P. Dorsey, and D. Emin, *Phys. Rev. Lett.* **78**, 951 (1997).